2012 NDIA GROUND VEHICLE SYSTEMS ENGINEERING AND TECHNOLOGY SYMPOSIUM
MODELING & SIMULATION, TESTING AND VALIDATION (MSTV) MINI-SYMPOSIUM
AUGUST 14-16, MICHIGAN

A METHOD TO ACHIEVE HIGH FIDELITY IN INTERNET-DISTRIBUTED HARDWARE-IN-THE-LOOP SIMULATION

Tulga Ersal
Department of Mechanical Engineering
University of Michigan
Ann Arbor, MI

Mark J. Brudnak
CASSI-HMS
TARDEC
Warren, MI

Youngki Kim
Ashwin Salvi
Jason B. Siegel
Anna Stefanopoulou
Jeffrey L. Stein
Department of Mechanical Engineering
University of Michigan
Ann Arbor, MI

Zoran Filipi
Department of Automotive Engineering
Clemson University
Greenville, SC

ABSTRACT

One of the main challenges of co-simulating hardware-in-the-loop systems in real-time over the Internet is the fidelity of the simulation. The stochastic delay of the Internet may significantly distort the dynamics of the network-integrated system. This paper presents the development of an iterative learning control based approach to improve fidelity in such network-integrated systems. Towards this end, a new metric for characterizing fidelity is proposed first, which, unlike some existing metrics, does not require knowledge about the reference dynamics (i.e., dynamics that would be observed, if the system was physically connected). Next, using this metric, the problem of improving fidelity is formulated as an iterative learning control problem. Finally, the proposed approach is utilized in a case study, which shows that the proposed approach can significantly improve the fidelity in Internet-distributed hardware-in-the-loop simulation.

I. INTRODUCTION

The key benefit of hardware-in-the-loop (HIL) simulation is well known: it uniquely combines the advantages of physical prototyping and simulation-based engineering and thus allows for experiments that are at the same time cost effective and highly accurate [1]. It has therefore become indispensable in many application areas, such as automotive [2, 3], aerospace [4, 5], manufacturing [6], robotics [7, 8], and defense [9, 10].

Recently, Internet-distributed HIL simulation (ID-HIL) started attracting interest as a framework that enables concurrent system engineering even if the components that comprise the desired HIL setup are geographically distributed. This idea has found applications in the fields of earthquake engineering [11-16] and automotive engineering

[17-23], and is also closely related to teleoperation in robotics and haptics [24-31].

One of the key challenges in ID-HIL simulation is ensuring fidelity. In this context, fidelity refers specifically to how close the dynamics of the networked system are to the dynamics that would be observed if the system was physically integrated (i.e., reference dynamics). Several methods to characterize fidelity have been proposed in the literature. For example, a frequency-domain metric called distortion was proposed as the normalized difference between the networked and reference dynamics [32, 33]. In the telerobotics and haptics literature, many other frequency domain metrics are used, which could be adopted into the ID-HIL framework, as well [34-39]. A time-domain, statistical approach was also proposed to distinguish the inherent variation in the reference dynamics from the additional variation introduced due to the network [20, 23].

Several methods to improve fidelity have been proposed in the literature, as well. These methods include selecting appropriate coupling points [32, 33], using feedback control [40-42], and observer-based approaches [17-19]. The limitations of these techniques can be briefly summarized as follows. Coupling-point-based approaches work well if a coupling point with desired characteristics exists. However, such a coupling point may not always exist. Feedback-based techniques are subject to well-known fundamental trade-offs [41-43]; i.e., improving fidelity at one frequency compromises it at another frequency. Observer-based techniques rely on the existence of high-fidelity models. However, not having such models or avoiding the need to develop such models is the main motivation behind the HIL paradigm. Thus, improving fidelity in ID-HIL systems is still an open research question and is the focus of this paper.

In an effort to overcome the abovementioned limitations of the existing techniques, this paper proposes an iterative learning based approach to improving fidelity in ID-HIL systems. First, a new metric to characterize fidelity is proposed. Unlike some of the existing metrics, e.g. [20, 23, 32, 33], this metric does not require knowledge about the reference dynamics to quantify fidelity. Next, the fidelity-improvement problem is formulated as an iterative learning control problem. Finally, the proposed formulation is applied to an ID-HIL case study that highlights the potential performance of the proposed approach.

II. CHARACTERIZING FIDELITY

As mentioned in Section I, many metrics have been proposed to characterize fidelity, especially in telerobotics and haptic systems. There are two fundamental barriers to adopting the existing metrics to the ID-HIL framework: (1) Most of these metrics have been developed in a linear and deterministic framework. However, ID-HIL systems are, in general, nonlinear and stochastic. (2) Most of the existing metrics assume that the desired system dynamics are known and utilize this knowledge as a benchmark to measure the fidelity of the networked system. The benchmark for an ID-HIL system would be a physical assembly of the system. However, the main motivation of the ID-HIL paradigm is the lack of availability of a physical assembly. Thus, even though the existing metrics could still be helpful in a research environment where a physical assembly could be made available to develop and test ID-HIL techniques, in practice the desired system dynamics are unknown and most of the existing fidelity metrics cannot be defined.

Therefore, the aim of this section is to characterize fidelity in an ID-HIL system despite the lack of knowledge about the dynamics that the ID-HIL system is to emulate as accurately as possible. Towards this end, this work uses the error between the instantaneous values of coupling signals at both ends of the network.

To explain this idea, consider the example two-site ID-HIL framework shown in Fig. 1. Systems 1 and 2, both of which may include hardware and models, are integrated over a network through the coupling variables c_1 and c_2.

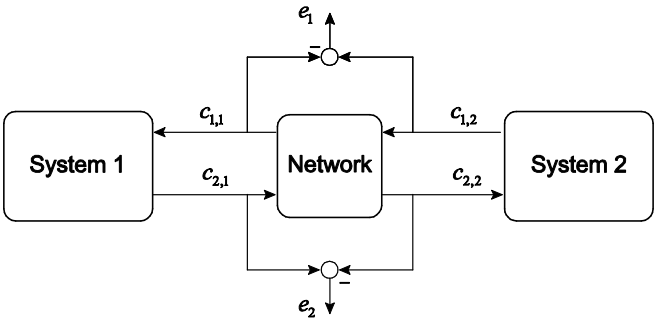

Figure 1: Illustration of an ID-HIL system with two sites (System 1 and 2). The variable $c_{i,j}$ represents the *i*-th coupling variable on the System *j* side of the network. The variable e_i represents the instantaneous error in the *i*-th coupling variable and is used to characterize fidelity.

Due to the numerous considerations associated with integration over a network (e.g., network delays, communication bandwidth, filters, sampling, etc.), the instantaneous value of the coupling variable i will not be the same on the two sides of the network. Let $c_{i,j}(t)$ represent the value of c_i as seen by System j at time t. Ideally, i.e., if the systems were co-located and coupled physically, we would have $c_{i,1}(t) = c_{i,2}(t)$. In the ID-HIL case, however, the two instances of the variable are not the same, i.e., $c_{i,1}(t) \neq c_{i,2}(t)$. Thus, we propose to use the difference between $c_{i,1}$ and $c_{i,2}$ as a metric for fidelity in the coupling variable i; i.e.,

$$\begin{aligned} e_1(t) &= c_{1,2}(t) - c_{1,1}(t), \\ e_2(t) &= c_{2,1}(t) - c_{2,2}(t). \end{aligned} \tag{1}$$

Note that causality is taken into account while defining the error signals in (1) when using the system output instances of the variables (i.e., $c_{1,2}$ and $c_{2,1}$) as the references for the system input instances of the same variables (i.e., $c_{1,1}$ and $c_{2,2}$).

It must also be emphasized that increasing fidelity of one of the coupling signals does not automatically imply an increase in the fidelity of the remaining coupling signals, as shown in [32, 33]. Thus, in general, no single coupling signal error can completely describe the system fidelity by itself. Therefore, to increase the *system* fidelity, this error needs to be driven to zero for *all* coupling variables, even though the needed amount of reduction in error may not be the same for all coupling variables. With respect to Fig. 1, for example, this implies $e_1 := c_{1,2} - c_{1,1} \to 0$ and $e_2 := c_{2,1} - c_{2,2} \to 0$.

To characterize *system* fidelity, all coupling signal errors can be aggregated into a single error metric. One way to achieve this is to use the following norm of weighted error norms:

$$E := \sqrt{\sum_{i=1}^{n} \left(w_i \left\| e_i \right\|_2 \right)^2}. \tag{2}$$

where n is the total number of coupling signals. The goal of maximizing the system fidelity then translates to minimizing the system-level error metric E.

The rationale behind using different weights for different error vectors is that the error in one coupling signal may be more critical than the error in another for a particular output of interest. In this paper, we will consider the weight

$$w_i = \frac{1}{\left\| e_i^0 \right\|_2}; \tag{3}$$

i.e., the norm of error of each coupling variable will be normalized with respect to its own initial value.

III. IMPROVING FIDELITY USING ITERATIVE LEARNING CONTROL

The fundamental problem with the proposed fidelity metric is that it is not available online; i.e., the value of $c_{i,1}$ and $c_{i,2}$ at a given instant cannot be made available for the error calculation at the same instant. The error $e_i(t)$ can be known only at $t + \tau$, i.e., after some delay τ that is needed to transmit the measurements $c_{i,1}(t)$ and $c_{i,2}(t)$ to the location where the error is calculated. Thus, the error cannot be used without delay to make online corrections to improve fidelity while an experiment is running. Even though the signal could be made available with a delay, so that a feedback loop could be closed around it, since the

overarching goal of this effort is to go beyond the fundamental limitations of such feedback methods, this option will not be discussed any further in this paper.

Instead, this work considers an offline application of the described metric to improve fidelity. To achieve this, the iterative learning control (ILC) paradigm is leveraged to improve fidelity of an ID-HIL experiment iteratively. The rest of this section describes this framework.

The ILC-based framework used in this work is illustrated in Fig. 2 for one of the coupling signals as an example. The error as defined in Eq. (1) is provided offline as the error signal to the ILC algorithm. Together with the control input used in the corresponding run, the algorithm then shapes the control input according to a learning algorithm to attenuate the error in the next run, i.e.,

$$\mathbf{u}_i^{m+1} = \mathbf{f}\left(\mathbf{u}_i^m, \mathbf{e}_i^m\right), \tag{4}$$

with

$$\begin{aligned} \mathbf{u}_i^m &= \begin{bmatrix} u_i^m(0) & u_i^m(1) & \cdots & u_i^m(N) \end{bmatrix}^T, \\ \mathbf{e}_i^m &= \begin{bmatrix} e_i^j(0) & e_i^m(1) & \cdots & e_i^m(N) \end{bmatrix}^T, \end{aligned} \tag{5}$$

where the superscript m is an index for the iteration, and N represents the number of time steps.

It is very important to emphasize here that this problem is not as trivial as using the error from the initial run and adding it to the coupling variable in the current run. The reason is the bidirectional nature of the coupling between the systems, which prevents the applicability of this trivial solution. For example, referring to the example in Fig. 2, any modification to $c_{1,1}^{m+1}(k)$ will propagate through System 1, Network, and System 2 and affect $c_{1,2}^{m+1}(n)$, $n = k+1, k+2, \ldots, N$. In other words, if $c_{1,2}$ is regarded as a reference for $c_{1,1}$ in the ILC framework, then the problem can be considered as the reference signal changing as a result of the ILC action.

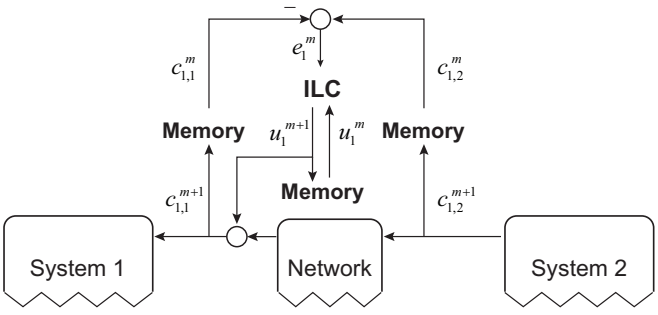

Figure 2: Proposed ILC-based framework for iteratively improving ID-HIL fidelity. This figure illustrates a decentralized approach in which an independent ILC controller is utilized for each coupling signal.

Thus, designing the learning function $\mathbf{f}\left(\mathbf{u}_i^m, \mathbf{e}_i^m\right)$ properly is crucial. Different learning functions could be considered for their suitability to ID-HIL. In this paper, the ILC learning algorithm of the form

$$u_i^{m+1}(k) = Q(q)\left(u_i^m(k) + L(q)e_i^m(k+1)\right) \tag{6}$$

is considered, since it was reported to be a widely used algorithm [44]. In (6), q represents the forward time shift operator. Due to their applicability to nonlinear systems and wide use [44], PD-type learning functions are considered here, e.g.,

$$u_i^{m+1}(k) = u_i^m(k) + k_p e_i^m(k) + k_d\left(e_i^m(k) - e_i^m(k-1)\right) \tag{7}$$

This type of learning functions also has the advantage of not requiring a model of the system as part of the design process [45-54], which is particularly suitable for the ID-HIL paradigm and the specific goals of this paper.

This ILC-based framework is applied to each coupling signal independently. In this framework, each coupling signal has its own ILC controller (with its own learning function) that does not communicate with the ILC controllers of the remaining coupling signals. Through such a decentralized approach, scalability can be achieved. In other words, even though the method is explained on a single coupling point in a two-site system, it readily extends to ID-HIL setups with multiple sites, as well.

IV. CASE STUDY DESCRIPTION

To investigate the viability of the framework described in Sections II and III, a case study is performed with a series-hybrid Mine Resistant Ambush Protected All-Terrain Vehicle (M-ATV). Some of the specifications of the vehicle platform considered are summarized in Table 1. A high-level overview of the system is shown in Fig. 3. Each shaded area in the figure corresponds to a different geographic location, and the dashed lines represent communications over the network. The engine and the battery are the hardware components, whereas the rest of the vehicle is simulated.

The details of the components that comprise the system are given next.

The Engine-in-the-Loop Setup

The hardware component of interest for this work is a Navistar 6.4L V8 diesel engine with 260 kW rated power at 3000 rpm and a rated torque of 880 Nm at 2000 rpm. It is intended for a variety of medium-duty truck applications covering the range between classes IIB and VII, and features technologies such as high pressure common rail fuel injection, twin sequential turbochargers, and exhaust gas recirculation. A high-fidelity AC electric dynamometer couples the physical engine with the simulation models in real time and operates in speed control mode. The setup can be connected to Simulink for integration with mathematical models, allowing for a real-time hardware-in-the-loop simulation. This connection is achieved through an EMCON 400 flexible test bed with an ISAC 400 extension [55]. The photo of the setup is shown in Fig. 4.

Table 1. Vehicle specification

Component	Specification
Vehicle	Hybridized Mine Resistant Ambush Protected All-Terrain Vehicle (M-ATV)
Weight	14,403 kg
Payload	1814 kg
Frontal Area	5.72 m^2
Engine	6.4L V8 turbo-diesel: 260 kW
Generator	Permanent Magnet: 265 kW
Battery	Lithium Iron Phosphate: 9.87 kWh

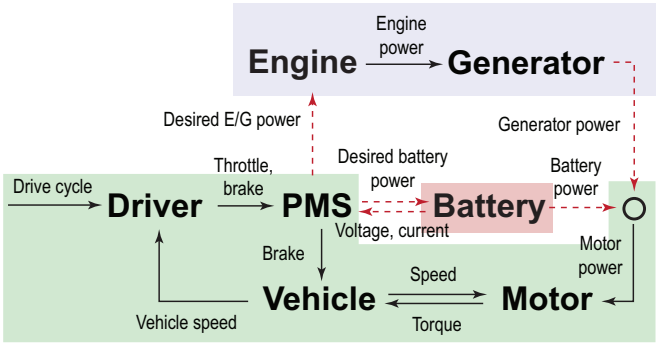

Figure 3: The overview of the system considered in this case study.

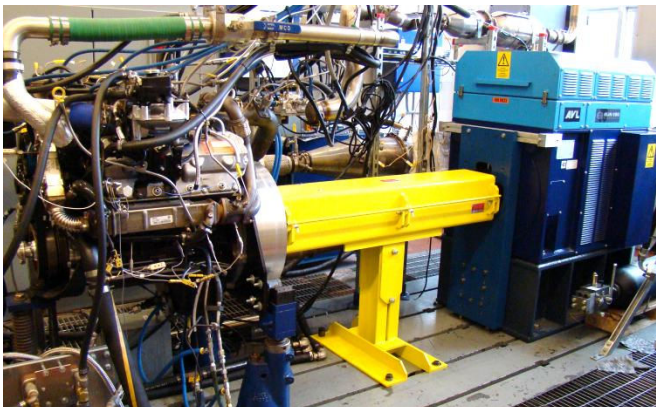

Figure 4: A photo of the engine-in-the-loop testing facility

Motor/Generator Model

The motor and the generator are modeled using quasi-steady state efficiency maps under assumption that their dynamics are much faster than vehicle dynamics and transients are negligible. As shown in Fig. 5, the efficiency of the electric machine (EM) η_{EM} is expressed as a function of electrical torque T_{EM} (or electrical Power P_{elec}) and speed ω_{EM}:

$$P_{\mathrm{mech}} = P_{\mathrm{elec}} \eta_{\mathrm{EM}}^{\ k}, \tag{8}$$

$$\eta_{\mathrm{EM}} = \eta_{\mathrm{EM}}\left(\omega_{EM}, T_{\mathrm{EM}}\right), \tag{9}$$

$$\eta_{EM} = \eta_{EM}\left(\omega_{EM}, P_{\mathrm{elec}}\right), \tag{10}$$

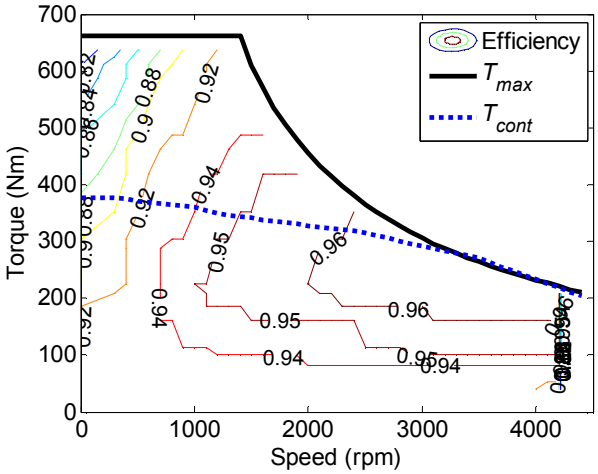

Figure 5: Efficiency contour map of an electric motor superimposed by maximum and continuous torque

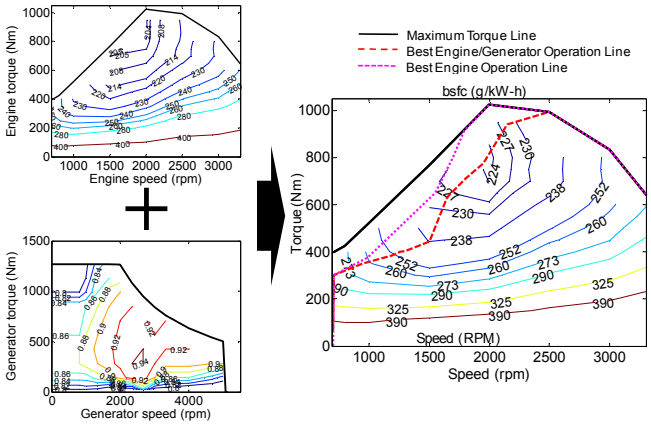

Figure 6: *bsfc* of engine/generator unit obtained by combining engine *bsfc* and generator efficiency and superimposed by optimal operation lines of the engine/generator unit and the engine only

where P_{mech} is mechanical power and k indicates the direction of power flow: $k=1$ represents that electrical power is converted to mechanical power, and $k=-1$ means that the mechanical power is converted to electrical power. Maximum output torque of the motor $T_{\max}$ is governed between the continuous torque curve and the peak torque curve accounting for the heat index α as follows:

$$T_{\max} = \alpha T_{\text{cont}} + (1-\alpha) T_{\text{peak}}, \qquad (11)$$

$$\alpha = -0.3 - \int \frac{0.3}{\tau_{EM}} \left(\frac{T_{EM}}{T_{\text{cont}}} \right) dt, \qquad (12)$$

where T_{peak} and T_{cont} are the peak and continuous torque respectively, and these torques are a function of the motor speed (Fig. 7). The heat index varies from zero to one and is used to emulate the change in the torque limit based on motor temperature. The time constant τ_{EM} of 180 seconds is selected in *Powertrain systems analysis toolkit* developed by Argonne National Laboratory.

Optimal Engine/Generator Operation

The best efficient operating points of engine/generator combined system are different from the best engine-efficient operating points. In a series hybrid configuration, the attached generator possibly shifts the best fuel efficient operating points of the combined system to other operating points. The combined system brake specific fuel consumption (*bsfc*) map is obtained by dividing the engine *bsfc* map is divided by the generator efficiency map. The *bsfc* of the engine/generator unit $bsfc_{eng/gen}$ can be calculated by using

$$bsfc_{eng/gen} = bsfc_{eng}/\eta_{gen}\,. \qquad (13)$$

The best fuel-efficient operating line is then determined by searching the minimum fuel consumption point for any given power demand. Figure 6 shows the combined $bsfc_{eng/gen}$ and optimal operation line of the engine/generator unit which is used in this study.

The Battery-in-the-Loop Setup

The Battery Testing Laboratory employed in this case study is equipped with a Bitrode Model FTV1 battery cycler that has a voltage range of 0-60V for 1-12 batteries in series, offers three current ranges (0-2A, 0-20A, and 0-200A) and a 10 ms control and data acquisition rate. A Cincinati-Sub-Zero Model ZPH-16-3.5-SCT/AC temperature and humidly test chamber has a volume of 453 L that can accommodate a battery

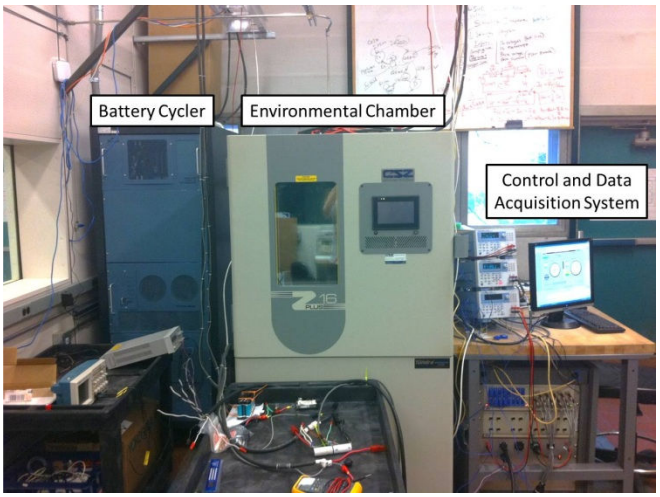

Figure 7: The battery testing laboratory

pack, and offers a temperature range of -45°C to 190°C, and a humidity range of 10% to 98% RH.

A single cylindrical A123 26650 $LiFePO_4$ battery with the capacity of 2.3Ah is used for the testing. The voltage and current of the single cell is scaled up to represent the corresponding values for the battery pack.

A photo of the battery laboratory is shown in Fig. 7.

Vehicle Dynamics Model

The longitudinal dynamics of the vehicle is calculated by using

$$M_{\text{veh}} \frac{dv_{\text{veh}}}{dt} = F_{\text{prop}} - F_{\text{RR}} - F_{\text{WR}} - F_{\text{GR}} - F_{\text{brk}}, \quad (14)$$

where M_{veh} and v_{veh} are the mass and velocity of the vehicle respectively, F_{prop} is the propulsion force, and F_{RR} is the rolling resistance force expressed by

$$F_{\text{RR}} = f_r M_{\text{veh}} g \cos\theta, \quad (15)$$

where f_r is rolling resistance, g is gravitational acceleration, and θ is the road grade. The wind resistance force F_{WR} is calculated by using

$$F_{\text{WR}} = \frac{1}{2} \rho_{\text{air}} C_d A_{\text{veh}} v_{\text{veh}}^2, \quad (16)$$

where ρ_{air} is the air density, C_d is the drag coefficient, and A_{veh} is frontal area of the vehicle. The grade resistance force, $F_{\text{GR}} = M_{\text{veh}} g \sin\theta$, is set to zero in the driving cycles in this study.

Driver Model

The driver model takes the desired and actual vehicle velocities as inputs and acts on their difference through a proportional-integral (PI) control strategy to generate a control signal. This control signal is saturated to remain within [-1,1], where positive and negative values are interpreted as throttle and brake commands, respectively. The PI controller is also augmented with an anti-windup strategy to avoid integration windup when the control signal saturates.

Power Management Strategy

The power management strategy employed in this case study is a frequency domain power distribution strategy that splits the total power demand into low frequency and high frequency components. The low frequency demand is fed to the engine for a smooth operation, whereas the high frequency demand is fed to the battery for shallow battery operating range.

Figure 8 shows the structure of the proposed strategy consisting of: 1) FDPD module; 2) SOC regulation module; and 3) mode decision module.

The FDPD module for HEV mode determines the engine/generator power demand by splitting total power demand in low and high frequency ranges. The power demand before deciding a

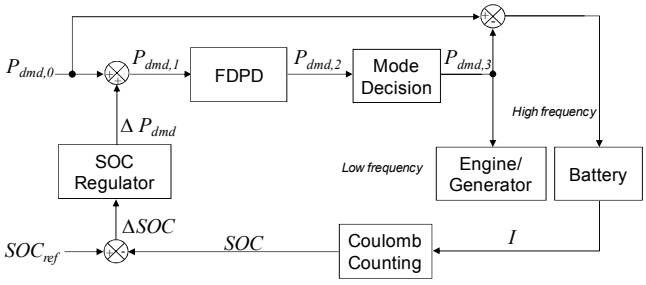

Figure 8: The schematic diagram of FDPD strategy

vehicle mode $P_{dmd,2}$ is determined by following steps:

if $P_{dmd,0} \geq P_{th1}$ and $P_{dmd,0} < P_{th2}$
$P_{dmd,1} = P_{dmd,0} + \Delta P_{dmd}$
else if $P_{dmd,0} \geq P_{th2}$
$P_{dmd,1} = P_{th2} + \Delta P_{dmd}$
else
$P_{dmd,1} = \Delta P_{dmd}$

$$\tau_{LF} \frac{dP_{dmd,2}}{dt} + P_{dmd,2} = P_{dmd,1}$$

where $P_{dmd,0}$ and $P_{dmd,1}$ are power demand for vehicle propulsion and total power demand respectively. P_{th1} and P_{th2} are threshold power levels for HEV mode incorporated with load-leveling, and τ_{LF} is the time constant of a low-pass filter. The feedback power demand ΔP_{dmd} for the battery SOC regulation is determined through the proportional-integral (PI) controller using the difference between the reference SOC, SOC_{ref} and current SOC

$$\Delta P_{dmd} = k_P \cdot \Delta \mathrm{SOC} + k_I \int \Delta \mathrm{SOC} dt \,, \qquad (17)$$

where k_P and k_I are proportional and integral gain respectively.

The mode decision module determines driving modes. The modes change between an electric-vehicle (EV) mode, a hybrid electric vehicle (HEV) mode and a performance vehicle (PV) mode as following:

if $P_{dmd,2} \leq P_{th1}$
$P_{dmd,3} = 0$: EV mode
if $P_{dmd,2} \geq P_{dmd,0} - P_{batt,max}$
$P_{dmd,3} = P_{dmd,2}$: HEV mode
else ($P_{dmd,2} < P_{dmd,0} - P_{batt,max}$)
$P_{dmd,3} = min(P_{eng,max}, P_{dmd,0} - P_{batt,max})$: PV mode

where $P_{eng,max}$ and $P_{batt,max}$ are maximum available engine power and battery discharging power respectively. Consequently, the performance of FDPD strategy is determined by five control parameters; namely, τ_{LF}, P_{th1}, P_{th2}, k_P, and k_I. These five parameters are determined through model-based multi-phase optimization process.

System Integration through the Network

The components described above were integrated over the network according to Fig. 3. All the communications happened over the local area network except for the desired battery power, which was routed through an off-campus computer using the Internet. This communication experienced an average delay of about 70ms. Figure 9 shows a representative illustration of the delays that the packets experienced during a network characterization test.

The ILC Framework

With respect to Fig. 2, the variable $c_{1,1}$ described the desired battery power on the battery side of the Internet, $c_{1,2}$ described the same quantity on the PMS side, and $e_1 = c_{2,1} - c_{1,1}$ captured the error between the two. The ILC framework aimed to reduce this error iteratively to improve the fidelity of the networked simulation according to a P-type learning function of the form

$$u_i^{m+1}(k) = u_i^m(k) + k_p e_i^m(k) \qquad (18)$$

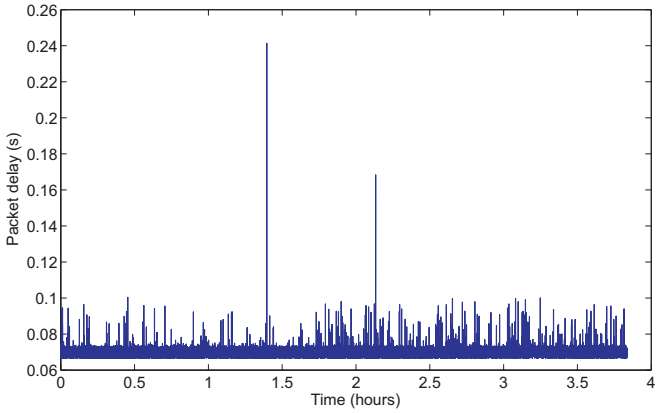

Figure 9: Packet delays observed during a network characterization test

V. CASE STUDY RESULTS

The networked vehicle system described in Section IV was simulated using a portion of the aggressive military driving cycle *Urban Assault Cycle* [56]. Frequent high acceleration and deceleration events create aggressive propulsion and braking situations. The velocity profile of this driving cycle is displayed Fig. 10. The parameters of the FDPD strategy are summarized in Table 3.

The trajectory of the error in the desired battery power through the ILC iterations is shown in Fig. 11. The figure shows that after 15 iterations, the proposed approach can achieve more than 70% reduction in the coupling variable error. It is worth noting that this number does not represent an upper limit on how much improvement can be achieved with this approach, because neither the ILC gains, nor the ILC learning function is optimized by any means. Nevertheless, this 70+% reduction in error is still representative of the levels of improvement in fidelity that can be achieved using the proposed technique.

Figure 12 illustrates what this 70+% improvement means in terms of the dynamics of the system. The figure illustrates a portion of the actual battery power trajectory and compares the dynamic response observed without and with the ILC framework to the dynamics that would be observed if the desired battery power was also communicated over the local area network with negligible delays. The oscillations that are observed in the response due to the Internet delays can be significantly attenuated by the ILC framework, improving the fidelity of the networked simulation.

These results highlight the merit and potential of the proposed framework to improve fidelity, and encourage the further development of this framework. Some specific questions of interest are what the system requirements are for the proposed

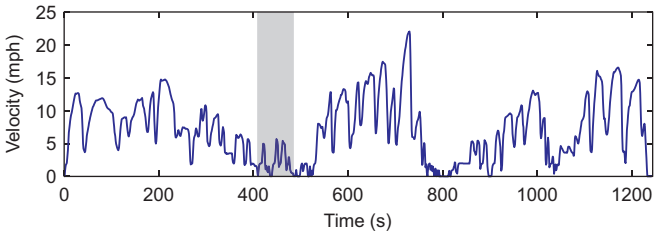

Figure 10: The speed profile of *Urban Assault Cycle*. The shaded region is used in this study.

Table 3. Optimized variables of the FDPD strategy

Variable	Value
Cut-off frequency, τ_{LF}	0.205
Threshold Power 1, P_{th1}	16.7 kW
Threshold Power 2, P_{th2}	116.7 kW
Proportional gain, k_P	836203.7
Integral gain, k_I	4537.0

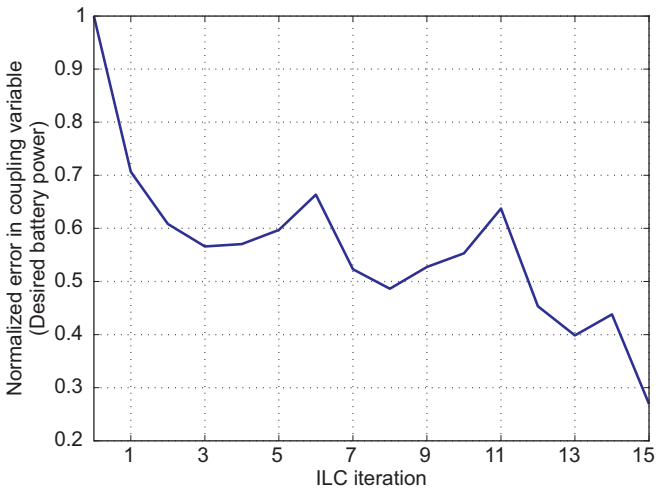

Figure 11: ILC performance

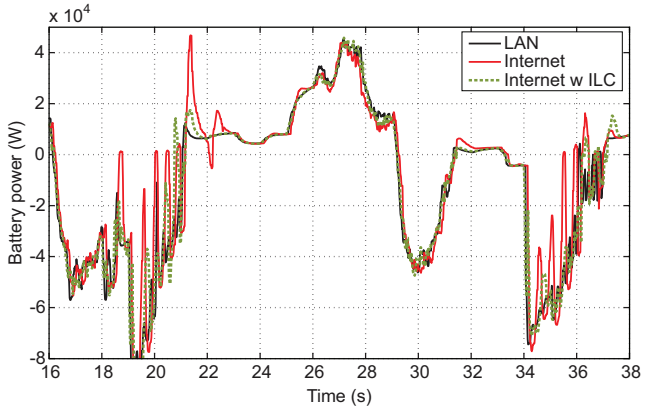

Figure 12: Battery power as a representative system response to illustrate how Internet delay can affect system dynamics and how the proposed method can alleviate its negative impact

framework to work, what type of learning functions are best suited for this application, how the ILC parameters relate to system characteristics, and what the robustness of this approach is and how it can be maximized. In terms of robustness, the robustness to variations in the initial conditions when actual hardware is introduced and the robustness to variations in the network delays are of particular importance. Potential future work also includes an investigation of the convergence properties and the trade-offs between a monotonic convergence and the error attenuation performance.

VI. SUMMARY AND CONCLUSIONS

An iterative learning control based framework has been developed to improve fidelity in Internet-distributed hardware-in-the-loop simulation. The framework has been tested using a case study that showed that more than 70% reduction in coupling variable errors can be obtained with the proposed method. The results imply that the framework can improve the fidelity of the networked simulation significantly, and encourage further development.

ACKNOWLEDGMENTS

This work was supported by the Automotive Research Center (ARC), a U.S. Army Center of Excellence in Modeling and Simulation of Ground Vehicles.

DISCLAIMER

Reference herein to any specific commercial company, product, process, or service by trade name, trademark, manufacturer, or otherwise, does not necessarily constitute or imply its endorsement, recommendation, or favoring by the United States Government or the Department of the Army (DoA). The opinions of the authors expressed herein do not necessarily state or reflect those of the United States Government or the DoA, and shall not be used for advertising or product endorsement purposes.

REFERENCES

[1] H. K. Fathy, Z. S. Filipi, J. Hagena, and J. L. Stein, "Review of hardware-in-the-loop simulation and its prospects in the automotive area," SPIE - Modeling and Simulation for Military Applications, Kissimmee, FL, United States, vol. 6228, pp. 1-20, SPIE, 2006.

[2] A. Kimura and I. Maeda, "Development of engine control system using real time simulator," 1996 IEEE International Symposium on Computer-Aided Control System Design, pp. 157-163, 1996.

[3] R. Verma, D. Del Vecchio, and H. K. Fathy, "Development of a scaled vehicle with longitudinal dynamics of an HMMWV for an ITS testbed," *IEEE/ASME Transactions on Mechatronics*, vol. 13, no. 1, pp. 46-57, 2008.

[4] J. Leitner, "A hardware-in-the-loop testbed for spacecraft formation flying applications," 2001 IEEE Aerospace Conference, vol. 2, pp. 615-620, IEEE, 2001.

[5] X. Yue, D. M. Vilathgamuwa, and K.-J. Tseng, "Robust adaptive control of a three-axis motion simulator with state observers," *IEEE/ASME Transactions on Mechatronics*, vol. 10, no. 4, pp. 437-448, 2005.

[6] A. Ganguli, A. Deraemaeker, M. Horodinca, and A. Preumont, "Active damping of chatter in machine tools - demonstration with a 'hardware-in-the-loop' simulator," *Journal of Systems and Control Engineering*, vol. 219, no. 5, pp. 359-369, 2005.

[7] F. Aghili and J.-C. Piedboeuf, "Contact dynamics emulation for hardware-in-loop simulation of robots interacting with environment," 2002 IEEE International Conference on Robotics and Automation, Washington, D.C., vol. 1, pp. 523-529, IEEE, 2002.

[8] G. D. White, R. M. Bhatt, C. P. Tang, and V. N. Krovi, "Experimental evaluation of dynamic redundancy resolution in a nonholonomic wheeled mobile manipulator," *IEEE/ASME Transactions on Mechatronics*, vol. 14, no. 3, pp. 349-357, 2009.

[9] J. A. Buford, Jr., A. C. Jolly, S. B. Mobley, and W. J. Sholes, "Advancements in hardware-in-the-loop simulations at the U.S. Army aviation and missile command," SPIE - Technologies for Synthetic Environments: Hardware-in-the-Loop Testing V, R. L. Murrer (ed., vol. 4027, pp. 2-10, SPIE, 2000.

[10] E. G. Huber Jr and R. A. Courtney, "Hardware-in-the-loop simulation at wright laboratory's dynamic infrared missile evaluator (DIME) facility," 1997 Technologies for Synthetic Environments: Hardware-in-the-Loop Testing II, vol. 3084, pp. 2-8, SPIE, 1997.

[11] S. Mahin, R. Nigbor, C. Pancake, R. Reitherman, and S. Wood, "The establishment of the nees consortium,"

2003 ASCE/SEI Structures Congress and Exposition: Engineering Smarter, pp. 181-182, American Society of Civil Engineers, 2003.

[12] B. F. Spencer, A. Elnashai, N. Nakata, H. Saliem, G. Yang, J. Futrelle, W. Glick, D. Marcusiu, K. Ricker, T. Finholt, D. Horn, P. Hubbard, K. Keahey, L. Liming, N. Zaluzec, L. Pearlman, and E. Stauffer, "The most experiment: Earthquake engineering on the grid," NEESgrid, Technical Report NEESgrid-2004-41, 2004.

[13] P. Pan, M. Tada, and M. Nakashima, "Online hybrid test by internet linkage of distributed test-analysis domains," *Earthquake Engineering and Structural Dynamics*, vol. 34, no. 11, pp. 1407-1425, 2005.

[14] B. Stojadinovic, G. Mosqueda, and S. A. Mahin, "Event-driven control system for geographically distributed hybrid simulation," *Journal of Structural Engineering*, vol. 132, no. 1, pp. 68-77, 2006.

[15] Y. Takahashi and G. L. Fenves, "Software framework for distributed experimental-computational simulation of structural systems," *Earthquake Engineering and Structural Dynamics*, vol. 35, no. 3, pp. 267-291, 2006.

[16] G. Mosqueda, B. Stojadinovic, J. Hanley, M. Sivaselvan, and A. M. Reinhorn, "Hybrid seismic response simulation on a geographically distributed bridge model," *Journal of Structural Engineering*, vol. 134, no. 4, pp. 535-543, 2008.

[17] M. Compere, J. Goodell, M. Simon, W. Smith, and M. Brudnak, "Robust control techniques enabling duty cycle experiments utilizing a 6-DOF crewstation motion base, a full scale combat hybrid electric power system, and long distance internet communications," *SAE Technical Paper,* 2006-01-3077, 2006.

[18] J. Goodell, M. Compere, M. Simon, W. Smith, R. Wright, and M. Brudnak, "Robust control techniques for state tracking in the presence of variable time delays," *SAE Technical Paper,* 2006-01-1163, 2006.

[19] M. Brudnak, M. Pozolo, V. Paul, S. Mohammad, W. Smith, M. Compere, J. Goodell, D. Holtz, T. Mortsfield, and A. Shvartsman, "Soldier/harware-in-the-loop simulation-based combat vehicle duty cycle measurement: Duty cycle experiment 2," Simulation Interoperability Workshop, Norfolk, VA, Simulation Interoperability Standards Organization (SISO), 2007.

[20] T. Ersal, M. Brudnak, J. L. Stein, and H. K. Fathy, "Variation-based transparency analysis of an internet-distributed hardware-in-the-loop simulation platform for vehicle powertrain systems," ASME Dynamic Systems and Control Conference, Hollywood, California, ASME, 2009.

[21] T. Ersal, M. Brudnak, A. Salvi, J. L. Stein, Z. Filipi, and H. K. Fathy, "Development of an internet-distributed hardware-in-the-loop simulation platform for an automotive application," ASME Dynamic Systems and Control Conference, Hollywood, California, ASME, 2009.

[22] T. Ersal, M. Brudnak, A. Salvi, J. L. Stein, Z. Filipi, and H. K. Fathy, "Development and model-based transparency analysis of an internet-distributed hardware-in-the-loop simulation platform," *Mechatronics*, vol. 21, no. 1, pp. 22-29, 2011.

[23] T. Ersal, M. Brudnak, J. L. Stein, and H. K. Fathy, "Statistical transparency analysis in internet-distributed hardware-in-the-loop simulation," *IEEE/ASME Transactions on Mechatronics*, vol. 17, no. 2, pp. 228-238 2012.

[24] R. L. Kress, W. R. Hamel, P. Murray, and K. Bills, "Control strategies for teleoperated internet assembly," *IEEE/ASME Transactions on Mechatronics*, vol. 6, no. 4, pp. 410-416, 2001.

[25] I. Elhajj, J. Tan, N. Xi, W. K. Fung, Y. H. Liu, T. Kaga, Y. Hasegawa, and T. Fukuda, "Multi-site internet-based tele-cooperation," *Integrated Computer-Aided Engineering*, vol. 9, no. 2, pp. 117-127, 2002.

[26] S. Munir and W. J. Book, "Internet-based teleoperation using wave variables with prediction," *IEEE/ASME Transactions on Mechatronics*, vol. 7, no. 2, pp. 124-133, 2002.

[27] G. Niemeyer and J.-J. E. Slotine, "Toward bilateral internet teleoperation," in *Beyond webcams: An introduction to online robots*: MIT Press, 2002, pp. 193-213.

[28] L.-N. Sun, X.-H. Xie, L.-X. Fu, and Z.-J. Du, "Internet-based telerobotic surgery: Problems and approaches," *Harbin Gongye Daxue Xuebao/Journal of Harbin Institute of Technology*, vol. 35, no. 2, pp. 129-133, 2003.

[29] Y.-H. Shi and Y.-C. Wang, "Study on internet-based force feedback technology," *Robot*, vol. 26, no. 4, pp. 330-335, 2004.

[30] E. Slawinski, J. F. Postigo, and V. Mut, "Bilateral teleoperation through the internet," *Robotics and Autonomous Systems*, vol. 55, no. 3, pp. 205-215, 2007.

[31] N. Chopra, P. Berestesky, and M. W. Spong, "Bilateral teleoperation over unreliable communication networks," *IEEE Transactions on Control Systems Technology*, vol. 16, no. 2, pp. 304-13, 2008.

[32] T. Ersal, R. B. Gillespie, M. Brudnak, J. L. Stein, and H. K. Fathy, "Effect of coupling point selection on distortion in internet-distributed hardware-in-the-loop simulation," *International Journal of Vehicle Design*,

vol. Special Issue on Modeling and Simulation of Ground Vehicle Systems, in press.

[33] T. Ersal, R. B. Gillespie, M. Brudnak, J. L. Stein, and H. K. Fathy, "Effect of coupling point selection on distortion in internet-distributed hardware-in-the-loop simulation," American Control Conference, San Francisco, CA, USA, 2011.

[34] D. A. Lawrence, "Stability and transparency in bilateral teleoperation," *IEEE Transactions on Robotics and Automation*, vol. 9, no. 5, pp. 624-637, 1993.

[35] K. Hashtrudi-Zaad and S. E. Salcudean, "Transparency in time-delayed systems and the effect of local force feedback for transparent teleoperation," *IEEE Transactions on Robotics and Automation*, vol. 18, no. 1, pp. 108-114, 2002.

[36] K. B. Fite, J. E. Speich, and M. Goldfarb, "Transparency and stability robustness in two-channel bilateral telemanipulation," *Transactions of the ASME. Journal of Dynamic Systems, Measurement and Control*, vol. 123, no. 3, pp. 400-7, 2001.

[37] M. C. Çavuşoğlu, A. Sherman, and F. Tendick, "Design of bilateral teleoperation controllers for haptic exploration and telemanipulation of soft environments," *IEEE Transactions on Robotics and Automation*, vol. 18, no. 4, pp. 641-647, 2002.

[38] G. De Gersem, H. Van Brussel, and F. Tendick, "Reliable and enhanced stiffness perception in soft-tissue telemanipulation," *International Journal of Robotics Research*, vol. 24, no. 10, pp. 805-822, 2005.

[39] Y. Yokokohji and T. Yoshikawa, "Bilateral control of master-slave manipulators for ideal kinesthetic coupling - formulation and experiment," *IEEE Transactions on Robotics and Automation*, vol. 10, no. 5, pp. 605-619, 1994.

[40] Y. Yokokohji, T. Imaida, and T. Yoshikawa, "Bilateral teleoperation under time-varying communication delay," 1999 IEEE/RSJ International Conference on Intelligent Robots and Systems (IROS'99): Human and Environment Friendly Robots with High Intelligence and Emotional Quotients', vol. 3, pp. 1854-1859, IEEE, 1999.

[41] P. G. Griffiths, R. B. Gillespie, and J. S. Freudenberg, "A fundamental linear systems conflict between performance and passivity in haptic rendering," *IEEE Transactions on Robotics*, vol. 27, no. 1, pp. 75-88, 2011.

[42] P. G. Griffiths, R. B. Gillespie, and J. S. Freudenberg, "A fundamental tradeoff between performance and sensitivity within haptic rendering," *IEEE Transactions on Robotics*, vol. 24, no. 3, pp. 537-548, 2008.

[43] J. S. Freudenberg, C. V. Hollot, R. H. Middleton, and V. Toochinda, "Fundamental design limitations of the general control configuration," *IEEE Transactions on Automatic Control*, vol. 48, no. 8, pp. 1355-1370, 2003.

[44] D. A. Bristow, M. Tharayil, and A. G. Alleyne, "A survey of iterative learning control: A learning-based method for high-performance tracking control," *IEEE Control Systems Magazine*, vol. 26, no. 3, pp. 96-114, 2006.

[45] J.-X. Xu and Y. Tan, "Robust optimal design and convergence properties analysis of iterative learning control approaches," *Automatica*, vol. 38, no. 11, pp. 1867-1880, 2002.

[46] D. Wang, "On d-type and p-type ilc designs and anticipatory approach," *International Journal of Control*, vol. 73, no. 10, pp. 890-901, 2000.

[47] C.-C. Cheah and D. Wang, "Learning impedance control for robotic manipulators," *IEEE Transactions on Robotics and Automation*, vol. 14, no. 3, pp. 452-465, 1998.

[48] C.-J. Chien and J.-S. Liu, "A p-type iterative learning controller for robust output tracking of nonlinear time-varying systems," *International Journal of Control*, vol. 64, no. 2, pp. 319-334, 1996.

[49] G. Heinzinger, D. Fenwick, B. Paden, and F. Miyazaki, "Stability of learning control with disturbances and uncertain initial conditions," *IEEE Transactions on Automatic Control*, vol. 37, no. 1, pp. 110-114, 1992.

[50] K.-H. Park, Z. Bien, and D.-H. Hwang, "A study on the robustness of a pid-type iterative learning controller against initial state error," *International Journal of Systems Science*, vol. 30, no. 1, pp. 49-59, 1999.

[51] S. S. Saab, "Stochastic p-type/d-type iterative learning control algorithms," *International Journal of Control*, vol. 76, no. 2, pp. 139-148, 2003.

[52] R. Horowitz, "Learning control of robot manipulators," *Journal of Dynamic Systems, Measurement and Control, Transactions of the ASME*, vol. 115, no. 2 B, pp. 402-411, 1993.

[53] H. Havlicsek and A. Alleyne, "Nonlinear control of an electrohydraulic injection molding machine via iterative adaptive learning," *IEEE/ASME Transactions on Mechatronics*, vol. 4, no. 3, pp. 312-323, 1999.

[54] S. Arimoto, S. Kawamura, and F. Miyazaki, "Bettering operation of robots by learning," *Journal of Robotic Systems*, vol. 1, no. 2, pp. 123-140, 1984.

[55] Z. S. Filipi, H. K. Fathy, J. Hagena, A. Knafl, R. Ahlawat, J. Liu, D. Jung, D. N. Assanis, H. Peng, and J. L. Stein, "Engine-in-the-loop testing for evaluating hybrid propulsion concepts and transient emissions –

HMMWV case study," 2006 SAE World Congress, Detroit, MI, 2006.

[56] T.-K. Lee, Y. Kim, A. Stefanopoulou, and Z. S. Filipi, "Hybrid electric vehicle supervisory control design reflecting estimated lithium-ion battery electrochemical dynamics," 2011 American Control Conference, San Francisco, CA, USA, pp. 388-395, IEEE, 2011.